01 Jun 2020

Flow of Carbon Dioxide in Micro and Nano Pores and its Interaction with Crude Oil to Induce Asphaltene Instability

Sherif Fakher

Abdulmohsin Imqam

Missouri University of Science and Technology, ahikx7@mst.edu

Research Article

Flow of carbon dioxide in micro and nano pores and its interaction with crude oil to induce asphaltene instability

Sherif Fakher[1] · **Abdulmohsin Imqam**[1]

Received: 29 October 2019 / Accepted: 29 April 2020 / Published online: 8 May 2020

Abstract
This study presents an investigation of the flow mechanism of carbon dioxide (CO_2) through nano and micro pores and the impact of this flow on oil mobilization and asphaltene instability in the crude oil. The flow mechanism of CO_2 is determined using numerical modeling through the Knudsen number to determine the flow regimes under different thermodynamic conditions. Following this, the oil production and asphaltene stability are studied using a filtration vessel supplemented with nano and micron sized filter membranes. The effect of varying CO_2 injection pressure, oil viscosity, porous media pore size, and porous media thickness on oil mobilization and asphaltene stability are studied. Regarding the flow regimes, it is found that four distinct flows are observed during CO_2 injection in the nano and micro pores. These flow regimes included diffusion, transition, slippage, and viscous flow. As the pore size increases, the flow becomes viscous dominated. Crude oil flow through the nano pores required higher pressure and also resulted in more severe asphaltene damage and plugging compared to the micro pores. Increasing the CO_2 injection pressure increased oil production and decreased the asphaltene concentration in the bypassed crude oil, which is the oil remaining in the filtration vessel and could not be produced. The lower oil viscosity is associated with a lower asphaltene concentration and thus yields an overall higher oil viscosity as well. By undergoing this research, a better understanding of how the CO_2 flows through nano and micro pores can be achieved, and oil mobilization and asphaltene instability with time can also be understood.

Keywords Carbon dioxide flow · Micro and nano pores · Asphaltene instability

List of symbols

K_n	Knudsen number, dimensionless
λ	Mean molecular free path, m
L	Representative physical length, m
K_b	Boltzmann constant, J/K
T	Temperature, K
d	Particle hard shell diameter, m
p	Pressure, Pa
x	Distance, m
v_x	Velocity in x-direction, m/s
ρ	Fluid density, kg/m^3
β	Non-Darcy flow coefficient, D/Mscf
D_{Kn}	Knudsen diffusion, m^2/s
d_k	Pore throat radius, m
R_g	Universal gas constant, J/mol K
M	Molecular weight, Da
N_i	Molar flux, mol/cm^2 s
D_i	Diffusion coefficient, m^2/s
nm	Nanometer
μm	Micrometer

1 Introduction

During its injection in oil reservoirs, the CO_2 will propagate through the pores of the formation and interact with the crude oil in order to mobilize the oil and facilitate its production. Understanding the flow regimes by which CO_2

✉ Sherif Fakher, smfb96@mst.edu | [1]Missouri University of Science and Technology, Rolla, MO, USA.

flows in the pores of the formation is extremely important in order to determine how and where the CO_2 is most likely to go in the formation and thus determine the CO_2 oil production potential [1–5, 49–51]. CO_2 can result in asphaltene instability which may impact oil mobilization negatively along with causing severe problems in facilities and pipelines. It is extremely important to understand the effect that CO_2 has on asphaltene instability and how that may impact oil filtration.

Different methods have been used to model asphaltene and CO_2 flow in the reservoir and the flow regimes that may arise during its propagation through the pores. Shabro et al. [6] combined a new pore scale model with a reservoir simulation algorithm to model fluid flow while incorporating the effects of no-slip and slip flow, Knudsen diffusion, and Langmuir desorption. Okamoto et al. [7, 8] modeled fluids displacement mechanisms using Knudsen Number via molecular simulation. Negara et al. [9] investigated the effect of Knudsen diffusion on shale gas production behavior. Wu et al. [10] developed a model for bulk-gas transfer in nanopores dependent on slip flow and Knudsen diffusion. Xu et al. [11] studied free gas transport in nanopores of shale rocks through Knudsen diffusion using real gas equation of state and elastics hard-sphere model. Jin et al. [12] used the definition of the Knudsen Number to prove that the CO_2 flow in the nano-pores of the shale mainly falls under the Free Molecular Flow behavior, and is hence mainly governed by diffusion. Li et al. [13] established a gas-slip model for fluid movement in nanopores and determined the accuracy of the model using laboratory results by varying the Knudsen number and gas relative permeability. Lawal et al. [52] conducted an experimental study of asphaltene deposition in microcapillary tubes using a novel experimental setup. Based on their results, the pressure drop was found to be relatable to the permeability change of the tubes and the thickness of the asphaltene deposition layer. Elkhatib et al. [53] investigated deposition of asphaltene in flow lines using capillary tubes and scanning electron microscopy. The experimental results were then analyzed using a machine-learning algorithm. The asphaltene nanoaggregates had the highest affinity to surfaces of the capillary tubes. Boek et al. [54] researched asphaltene aggregation and deposition in capillary tubes using both experimental and simulation approaches. The simulation approach utilized stochastic rotation dynamics, while experiments analyzed asphaltene precipitation and deposition using optical microscopy. The experimental and simulation results were then matched to obtain information on flow conditions of crude oil that is associated with asphaltene instability. Ruiz-Morales and Mullins [55] used dissipative particle dynamics to model coarse-grained molecules at the mesoscale level, while taking into consideration the polycyclic aromatic hydrocarbon and the peripheral alkanes. Results showed that asphaltene molecules remained at the oil–water interface at an orientation perpendicular to the interface with a 45° tilt.

Asphaltene instability in different formations and lithologies has been studied by many researchers using different experimental and modeling techniques. Zendehboudi et al. [14] differentiated between precipitation, coming out of solution, and deposition, adhesion of the asphaltene to the rock. This helped provide a method by which to analyze asphaltene stages including precipitation, deposition, and flocculation [15–19]. Rassamdani et al. [20] observed another stage of asphaltene, referred to as asphaltene flocculation, where the asphaltene particles began forming clusters and aggregates of a large diameter size. Soroush et al. [21] studied asphaltene stability during CO_2 injection and determined that the state of asphaltene can actually impact asphaltene stability. Kalantari-Dahagi et al. [22] conducted one of the few studies that investigated asphaltene problems in carbonate reservoirs and found asphaltene to be extremely problematic at the bubble point. Shedid and Zekri [23] showed that with the increase in the rock permeability and average pore size, the asphaltene problems decreased significantly. This shows that studying the impact of pore size on asphaltene stability becomes extremely important. Tavakkoli et al. [24] attempted to model asphaltene precipitation using computer modeling and compared the results to those of the experimental results to investigate its accuracy. Yonebayashi et al. [25, 26] studied asphaltene instability using dynamic experiments in order to incorporate the electro-kinetic effect on asphaltene precipitation and deposition. Moradi et al. [27] investigated asphaltene instability in small micro pores using filter membranes with 0.2 µm pore size using nitrogen injection. Struchkov et al. [28] performed a detailed study formation damage due to asphaltene deposition in pores. The methodology utilized actual core plugs instead of filter membranes which makes their study extremely valuable. Results showed that asphaltene deposition will decrease the core permeability and thus may limit oil mobility and reduce the overall oil recovery. Shen and Sheng [29] researched asphaltene problems in shale reservoirs using Eagle Ford cores and nano filter membranes. Their research did not include the mechanism of asphaltene instability. Fakher and Imqam [30, 31] performed an extensive study of asphaltene behavior in nano pores and methods by which asphaltene can be mitigated. Mohammed et al. [32] conducted one of very few numerical modeling studies of asphaltene instability in small pore sized and attempted to reduce asphaltene damage without the use of chemical agents by relying on the injected fluid properties and the production method and schedule.

Understanding the mechanism by which CO_2 flows in oil reservoirs and studying the impact of CO_2 flow on asphaltene instability is extremely important both when modeling CO_2 flow and to avoid asphaltene operational problems during production. Even though several researchers have studied both topic using multiple methods, very few researchers have evaluated the effect of CO_2 flow regimes on asphaltene instability in both micro and nano pores together. This research extends the previous work conducted by Fakher et al. [19] which studied asphaltene instability visually and using some filtration studies. This research investigates CO_2 flow mechanisms, oil filtration, asphaltene buildup, and asphaltene content in both micro pores and nano pores in both the produced and the bypassed oil, which is the oil that was not produced, in order to provide a holistic view on the impact of some factors on CO_2 flow regimes, oil mobilization, and asphaltene instability in these pore sizes.

2 Experimental material

Filtration vessel a stainless steel high pressure filtration vessel was used to conduct all the experiments. The vessel housed both the crude oil and the CO_2.

Carbon dioxide CO_2 was supplied using a high pressure CO_2 cylinder. The flow of CO_2 was regulated using a pressure regulator attached to the cylinder.

Filter membranes filter membranes with 2.7 µm, 100 nm, 10 nm, and 0.2 nm pore size were used to conduct the filtration experiments and to study the flow regime.

Test tubes glass test tubes were used to collect the produced crude oil. Glass was used since plastic was found to interact with some of the components of the crude oil and the heptane used for the asphaltene quantification.

Crude oil crude oil with viscosity 469, 260.7, 119, and 63.7 cp were used to conduct the experiments. The crude oil was obtained from Kirk lease in Kansas. The 469 cp oil had an initial asphaltene concentration of 5.73 wt%. The crude oil was obtained from the separator with an initial viscosity of 469 cp. The viscosity was then reduced using different weight percent kerosene mixing. The kerosene was highly soluble in the crude oil.

3 Experimental setup

The experimental setup used to conduct the asphaltene stability experiments is shown in Fig. 1. The setup includes the CO_2 cylinder connected to a pressure regulator to control the flow from the cylinder and control the pressure value. The main filtration vessel includes the filter membrane, crude oil and CO_2. An O-ring is placed to prevent any leakages during the experiment. Also, a 60-micron mesh screen is added to prevent the filter membrane from rupturing at high pressure. The produced oil is collected at the outlet in a glass test tube for further analysis. The oil that remained in the filtration vessel and could not

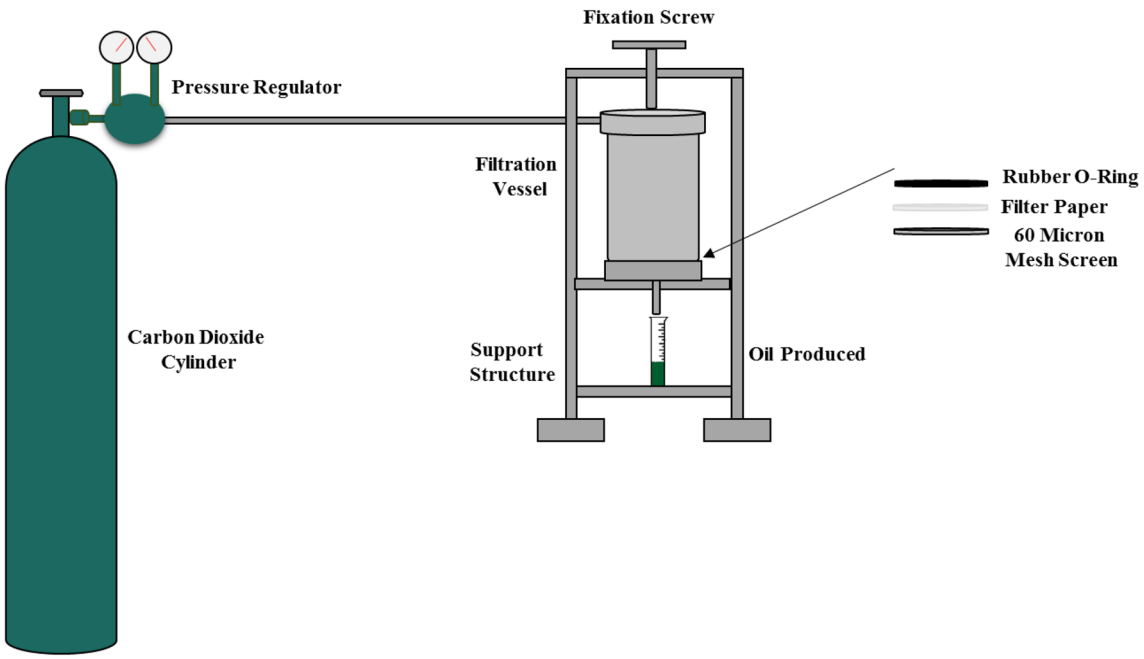

Fig. 1 Specially modified filtration setup

be produced was referred to as the bypassed oil and was also collected for analysis. The filtration vessel used differs slightly from the one used in our previous study [33]. The vessel used in this setup acquires a seal using a high vacuum rubber, while the other one is sealed using steel bolts. This is the main reason behind the difference in the sequence of the filter elements since the elements have to be in accordance with the rubber to avoid leakages during the filtration experiments.

4 Experimental procedure

The experimental procedure was based on initially preparing the crude oil sample to be tested, and then conduct the experiment. The procedure followed to conduct all the experiments is as follows:

- To prepare the filtration vessel, the bottom cap was detached, and then the 60 micron mesh screen was inserted into it. The mesh screen is a vital component of the setup since it provides a support base for the filter paper, and prevent is from rupturing during the experiment, while causing no hindrance to the flow since its pore size is much larger than that of the filter paper. The filter paper is then placed on top of the mesh screen, and then a rubber O-ring is placed on top of the filter paper. The O-ring ensures that a perfect seal is attained between the bottom cap assembly and the filtration vessel to avoid any potential for leaks during the experiment.
- After connecting the bottom cap, 100 ml of the specific viscosity oil used to run the experiment is poured into the filtration vessel. The top cap of the filtration vessel is then attached to the CO_2 cylinder, and fixed to the filtration vessel using the fixation screw on the top.
- The CO_2 cylinder is then opened, and the regulator is used to adjust the pressure to that of the experiment. The recording of the time commences as soon as the pressure regulator allows the release of the CO_2 to the setup.
- The oil production is recorded every 30 s for the first hour, and then every minute for the remaining duration of the experiment. The oil production flow rate is then calculated based on the produced volume and the time. The oil produced is collected for further analysis following the conclusion of the experiment.
- The CO_2 injection is maintained until CO_2 breakthrough occurs and no further oil production is observed.
- The bypassed oil, unproduced oil, is the collected from the vessel and stored for further analysis. The filter paper is also collected and stored in vacuum for further analysis.
- The asphaltene wt% in the produced oil and the bypassed oil is then calculated for each experiment to study the extent to which the asphaltene will plug the pores.
- The filter cake thickness and the area of asphaltene plugging on the filter paper is also calculated for each filter paper.
- In order to measure the weight of the asphaltene, the filter membrane bearing the asphaltene had to be dried initially. This was done by placing the filter membrane in a vessel with temperature of 80 °C. The membrane was maintained in the vessel for three days.
- Following this, the membrane was analyzed to ensure that it was completely dry and had no heptane in it. The filter membrane was then weighed in a scale with an accuracy of a 1000th of a gram.

5 Asphaltene detection test

Asphaltenes are defined as the heavy components of the crude oil that are insoluble in n-alkanes, such as n-heptane or n-pentane, but soluble in aromatics such as toluene or xylene [34]. It is important to determine if the crude oil used in this study has a percentage of asphaltene, and it is also crucial to quantify this asphaltene since it is a main operational problem during CO_2 flooding; the asphaltene detection and quantification test was run using the standard test for determination of asphaltenes (heptane insolubles) in crude petroleum (IP 143) [35]. It should be noted that the 0.45 µm membrane may bypass some of the asphaltene, especially for the smaller pore size experiment such as the 100, 10, and 0.2 nm experiments.

The procedure followed for the asphaltene detection test involved dissolving 0.1 ml of crude oil in 10 ml of n-heptane. The test tube is stirred vigorously for twenty seconds to ensure that the oil has been totally dissolved. The test tube is then set in an upright position for 48 h. Precipitation of the asphaltene will begin to become visible approximately one hour after the oil is dissolved, however the test tube must be left for at least 48 h to ensure that all the asphaltene has deposited from the solution. The asphaltene is then filtered from the solution using a 0.45 µm filter paper, and then the weight percent is calculated. The asphaltene is then dissolved in xylene, an aromatic, to ensure that all the precipitate was asphaltene and not any other component. The weight percent of the asphaltene was calculated using the equation below:

$$\text{Asphaltene wt\%} = \frac{\text{wt of asphaltene}}{\text{total wt of oil}} \times 100$$

6 Results and discussion

Both the CO_2 flow mechanism in nano and micro pores and the asphaltene deposition and precipitation will be discussed in this section. The CO_2 flow mechanism will include the CO_2 flow regimes identified using the Knudsen Number, the effect of varying CO_2 injection pressure, oil viscosity, pore size of the filter membrane, and filter membrane thickness. The asphaltene deposition and precipitation will include the asphaltene weight percent in both the produced oil and the unproduced oil and its effect on oil production.

6.1 CO_2 flow mechanism in nano and micro pores

6.1.1 Knudsen number

It is important to differentiate between the flow of CO_2 in conventional reservoirs and the flow of CO_2 in unconventional reservoirs. To be able to establish this differentiation, an understanding of the different flow regimes that could arise must be presented. The Knudsen number is considered one of the most applied and accurate indications of the type of flow that is occurring in the porous media [36–41]. The general form of the Knudsen number is presented.

$$K_n = \frac{\lambda}{L} = \left(\frac{K_b T}{\sqrt{2}\pi d^2 p} \right) / L \tag{1}$$

where K_n is the Knudsen number, λ is the mean molecular free path (m), L is the representative physical length which is the pore radius for this work (m), K_b is the Boltzmann constant (1.38065×10^{-23} J/k), T is the temperature (k), d is the particle hard shell diameter, or the diameter of the CO_2 molecule in this research (2.32×10^{-10} m), p is the pressure (Pa).

By using the Knudsen number, the flow regime for each pore size filter membrane can be identified for each of the CO_2 injection pressures used. Ziarani and Aguilera [36] defined four distinct flow regimes based on the value of the Knudsen number. These regions are defined in Fig. 2.

Viscous flow dominates the flow behavior in conventional hydrocarbon reservoirs. For viscous flow, Darcy's law can be applied safely given that the flow is laminar, which is usually represented by a low Reynolds number, usually close to unity. Viscous flow occurs at a Knudsen number below 0.01. If the flow becomes turbulent, such as in fractures or extremely high permeability formations or features, Forchheimer's equation becomes more applicable. Forchheimer's equation is shown [42].

$$\frac{dp}{dx} = \frac{-\mu}{k} v_x + \rho \beta {v_x}^2 \tag{2}$$

where p is the pressure, x is the distance, v_x is the velocity in x direction, ρ is the fluid density, and β is the non-Darcy flow coefficient of the porous medium.

During gas flow, the gas molecules will experience to some extent slippage at the pores' interface [43, 44]. This slippage becomes more profound as the permeability decreases, until a point where the gas slippage becomes overcome by diffusion in nano-pores. In the presence of gas, the conventional Darcy law can be applied, however a correction must be made to obtain representative values [43, 45]. This correction could either be the Klinkenberg correction or the Knudsen modification. Slip flow occurs for a Knudsen number value between 0.01 and 0.1.

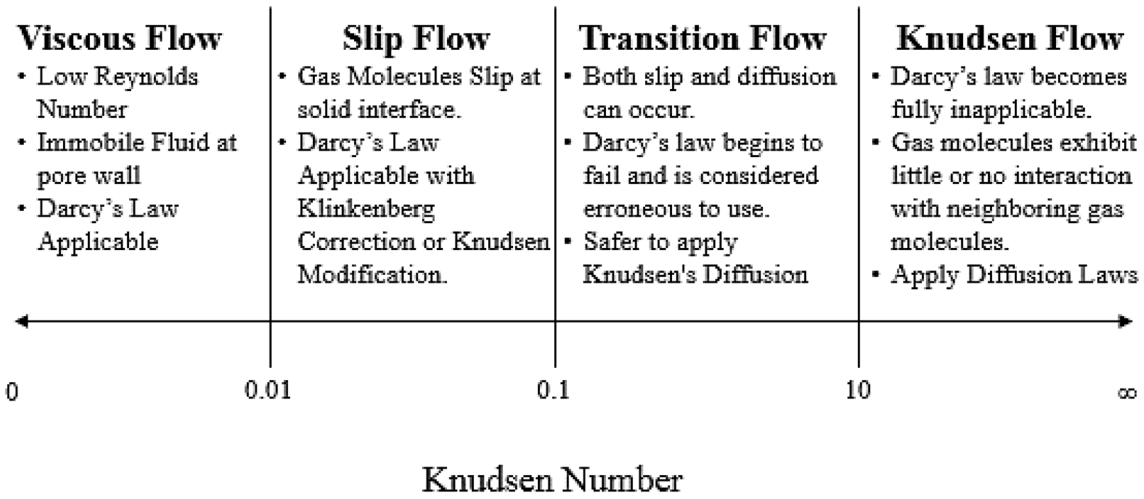

Fig. 2 Different flow regimes identified using Knudsen number

When the pore throats are decreased further beyond that of the slip flow, a transition flow occurs where both slip and diffusion flow occur. This occurs for a Knudsen number between 0.1 and 10. Even though Darcy's law has been applied to model flow during this flow regime, it usually produces erroneous results especially as the Knudsen number approaches 10. It is, therefore, safer to apply Knudsen's diffusion equation [36].

As the Knudsen number exceeds 10, the flow regime becomes Knudsen's Free Molecular flow. In this flow regime, Darcy's law becomes completely inapplicable, and diffusion based equations, such as Knudsen's diffusion, must be applied. In this type of flow, the gas molecules interact with the pore surface, and reach a point where there is almost no interaction between the gas molecules themselves [46]. This will occur mainly in the nano-pores of the unconventional shale reservoirs. Knudsen's diffusion equation is shown [38].

$$D_{\mathrm{Kn}} = \frac{d_k}{3}\sqrt{\frac{8R_{\mathrm{g}}T}{\pi M}} \tag{3}$$

where D_{Kn} is the Knudsen diffusion, d_k is the pore throat radius, R_g is the universal gas constant, M is the molecular weight, and T is the temperature.

If the pore size is extremely small, surface diffusion will be become predominant [47]. Surface diffusion is modeled using Fick's first law, shown.

$$N_{\mathrm{i}} = -D_i \nabla c_i \tag{4}$$

where N_i is the molar flux, D_i is the diffusion coefficient, and c_i is the concentration.

The Knudsen number was calculated for all the pore sizes used in this research at different pressures. Table 1 shows the Knudsen number values.

Based on these results, it is clear that the flow for all the experiments conducted using the 2.7 µm filter membranes is governed mainly using Darcy's law, with Klinkenberg correction in slip flow. When the filter membrane pore size decreases to the nano-meter scale, the flow becomes governed mainly by diffusion, modeled using Knudsen's diffusion or Fick's first law. This shows that the flow regime in the nano pores differs significantly form that of the micro pores, and hence there is a significant difference between the CO_2 flow behavior in unconventional and conventional reservoirs.

The flow mechanism study in this research has a specific applicability range based on the material used and the definition of the Knudsen number. The limitations of the flow mechanism study must therefore be mentioned and considered to avoid confusion. The main limitations of the flow mechanism methodology are as follow:

- The method does not consider heterogeneity or tortuosity.
- Since filter membranes are used, a longer porous media can such as cores can yield different results.
- The values used are for pure CO_2 and do not take into consideration other gases or mixtures.

6.1.2 CO_2 injection pressure

Three CO_2 injection pressures were used, including 25, 50, and 100 psi to study the effect of CO_2 injection pressure on the oil filtration, and the asphaltene deposition. The CO_2 when injected at different pressure will interact with the oil and flow through the pore spaces in a different manner. This difference in interaction and flow behavior results in both an effect on oil filtration, and oil flow, which was explained using the Knudsen number.

The effect of CO_2 injection pressure is shown in Fig. 3. Regardless of the oil viscosity, it is evident that as the CO_2 injection pressure increases, the oil production increases, and the CO_2 breakthrough time through the oil bank decreases. For example, regarding the 260.7 cp oil in Fig. 3b, the CO_2 breakthrough time for the 100 psi pressure was 480 s, or 8 min, with an oil production of 93% while the CO_2 breakthrough for the 25 psi was 2220 s, or 37 min, with an oil production of 91.5%.; even though this increment in oil production is not significant, in a real reservoir, compared to the filter membrane, the increment

Table 1 Knudsen number values and equivalent flow regimes for the experiments conducted

Pore size (L)	Pressure, Psi	Mean free PATH (λ), m	Knudsen number (λ/L)	Flow regime	Recommended equation
2.7 µm	25	9.84867×10^{-8}	0.03648	Slip flow	Darcy, with Klinkenberg
2.7 µm	50	4.92434×10^{-8}	0.01824	Slip flow	Darcy with Klinkenberg
2.7 µm	100	2.46217×10^{-8}	0.00912	Viscous flow	Darcy's Law
100 nm	300	8.20893×10^{-9}	0.082084	Slip flow	Darcy with Klinkenberg
10 nm	300	8.20893×10^{-9}	0.82084	Transition flow	Knudsen's Diffusion
0.2 nm	600	4.10347×10^{-9}	20.5174	Knudsen flow	Knudsen's Diffusion or Fick's Law

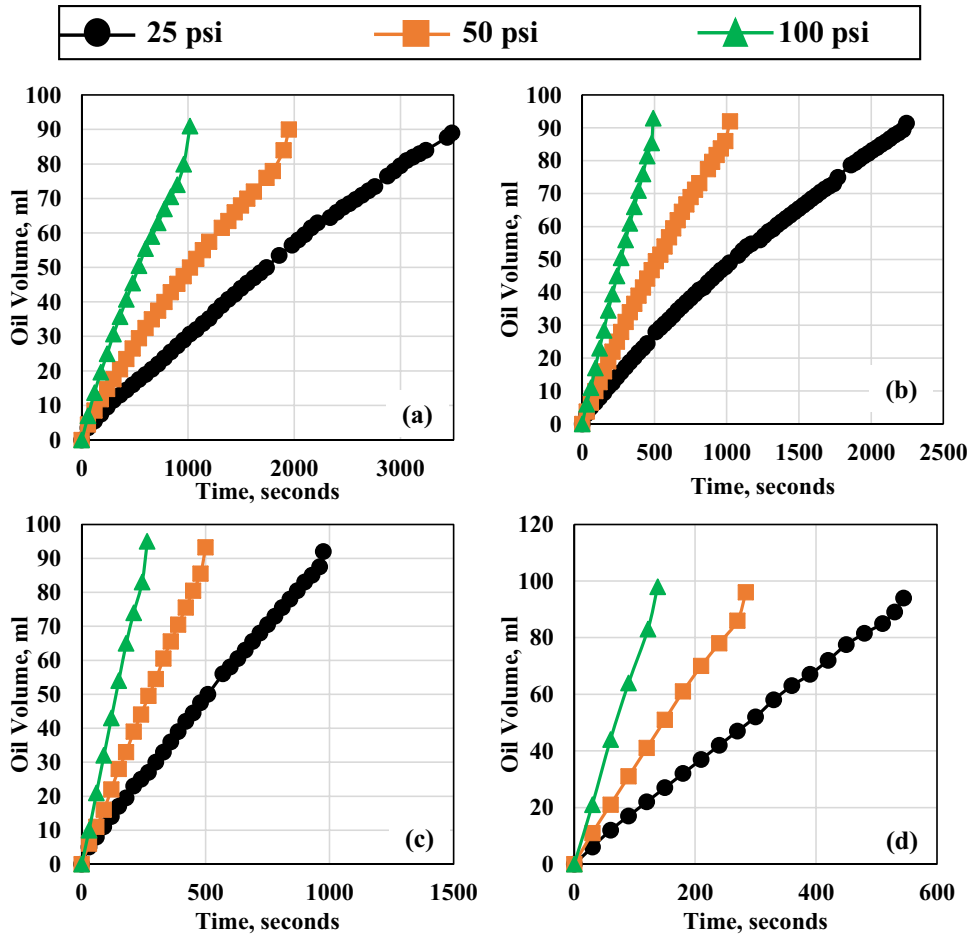

Fig. 3 Impact of varying CO_2 injection pressure on oil filtration for oil viscosities **a** 469 cp, **b** 260.7 cp, **c** 119 cp, **d** 63.7 cp

will be much higher. The oil production increase with the increase in CO_2 injection pressure was observed by several researchers, and is mainly attributed to the higher displacement of the oil due to the higher pressure [21–23].

The CO_2 could not produce all of the oil in the filtration vessel mainly due to its inability to mobilize the higher molecular weight components since they require larger pressure differentials to force them through the filter membranes. Even though there was a possibility to mobilize these components and force them through the micro-sized filter membranes, this possibility is eliminated in the nano-sized filter membranes.

The CO_2 breakthrough time is another significant parameter that was affected by the CO_2 injection pressure. From Fig. 3, the CO_2 breakthrough time is decreased significantly as the pressure increases. This shows that the CO_2 will produce all the oil that it is capable of mobilizing in a shorter duration compared to the lower CO_2 injection pressure. The CO_2 breakthrough time can be observed in the plots in Fig. 3 above as the data point before the last. The last data point shows a sudden increase in the oil filtration compared to the somewhat linear trend that the plots are following. This last data point is the oil filtration following CO_2 breakthrough. The sudden increase is due to the CO_2 mobilizing the last few milliliters of oil that it can after it has broken through. Due to the simultaneous production of the two fluids, including oil and CO_2, following this breakthrough, a more that usual oil volume is produced for a few seconds before production ceases. Other researchers also reported an increase in oil production after CO_2 breakthrough, which was a main contributor to the increase in the overall oil production percentage.

6.1.3 Oil viscosity

The oil viscosity is one of the main contributors to the oil filtration, and also one of the main factors that will impact asphaltene equilibrium in the oil and their precipitation and deposition. It was therefore paramount to investigate the viscosity's effect on oil filtration and asphaltene deposition.

For the 2.7 µm filter membrane, four different viscosities were used in this study, including 469 cp, 260.7 cp, 119 cp, 63.7 cp. Four experiments were conducted for three different CO_2 injection pressures to study the impact of oil viscosity at different CO_2 injection pressures. Figure 4

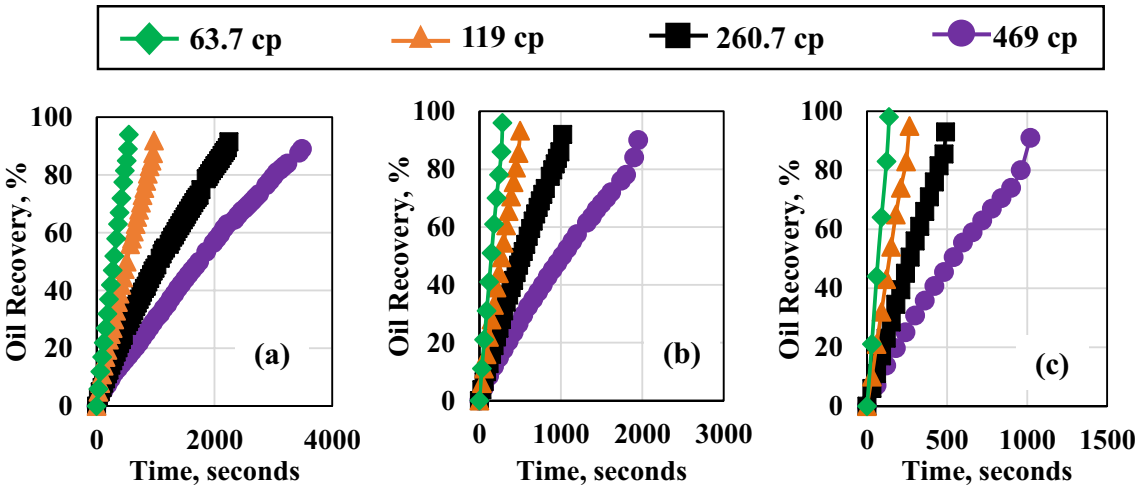

Fig. 4 Impact of varying oil viscosity on production using **a** CO_2 injection pressure 25 psi, **b** CO_2 injection pressure 50 psi, **c** and CO_2 injection pressure 100 psi

shows the results for all the oil viscosities at different CO_2 injection pressures.

When the oil viscosity was reduced for all the CO_2 injection pressures, the oil production increased. This is due to two main reasons. The first is that the decrease in oil viscosity makes it more prone to be mobilized by the CO_2, even at lower pressures. This in turn results in both a higher, and more rapid oil production, which can also be seen in Fig. 4. Lower viscosity oils required less time to produce the oil compared to the higher viscosity oils. The second reason is related to the asphaltene in the oil. As the viscosity of the oil is reduced, the overall asphaltene weight percent in the oil is also reduced, and therefore a smaller amount of oil is left behind, as will be clearly shown in the asphaltene weight percentages section. For example, in Fig. 4a, the oil production for the 469 cp oil took 3485 s, or 58 min to produce, whereas the 63.7 cp oil only took 530 s, or 8.8 min to produce. The asphaltene wt% for the 469 cp oil was found to be 5.73%, compared to 3.22% in the 63.7 cp oil. It is also important to point out that the values for the oil production are extremely high in all the experiments mainly due to the use of the filter membranes rather than a long porous media.

6.1.4 Porous media pore size

Four pore sizes were used in this research, including 2.7 µm, 100 nm, 10 nm, and 0.2 nm. It was identified earlier, using Knudsen Number, that the flow regime was different for different pore sizes. This section compares different pore sizes in terms of oil production, and oil production rate to further emphasize the difference between CO_2 flow in different pore sizes.

A comparison between the oil production, and the oil production flow rate for the 10 nm, and 100 nm is shown in Fig. 5. The 2.7 µm was not included in the comparison since the experiments were run at a different pressure. Also, the 0.2 nm will be explained separately since its results were different.

Both the 10 nm and the 100 nm experiments were conducted at 300 psi using a 100 ml initial volume. The total time until gas breakthrough was much longer for the 10 nm pore size membrane compared to the 100 nm membrane due to fluid being much more difficult to pass through the smaller pore size. The oil production for the 10 nm membrane appears to be larger compared to the 100 nm membrane. At the experimental conditions, crude oil will not be impacted significantly by CO_2 dissolution. This was studied in detail by Lobanov et al. [48] who showed experimentally that when CO_2 completely dissolved in the crude oil at 10wt% CO_2, the crude oil hardly swelled at all. The asphaltene many have played a role in varying the crude oil production however no conclusive reason can be reached with only the oil recovery data. The experiments were repeated two more times with the overall trend being the same. Also, when compared to the 2.7 µm filter membrane results, the oil production from the nano-membranes was reduced mainly due to the difference in the flow regime, and the inability to mobilize the majority of the asphaltene and heavy molecular weight components. The oil production flow rate indicated a longer time until stable flow rate for the 10 nm compared to the 100 nm which gives an indication of a larger filter cake thickness formation time for the smaller pore size. All in all, both the 100 nm and the 10 nm follow the same trend with a difference in oil production and oil flow rate stability time due to the difference in pores size. This same

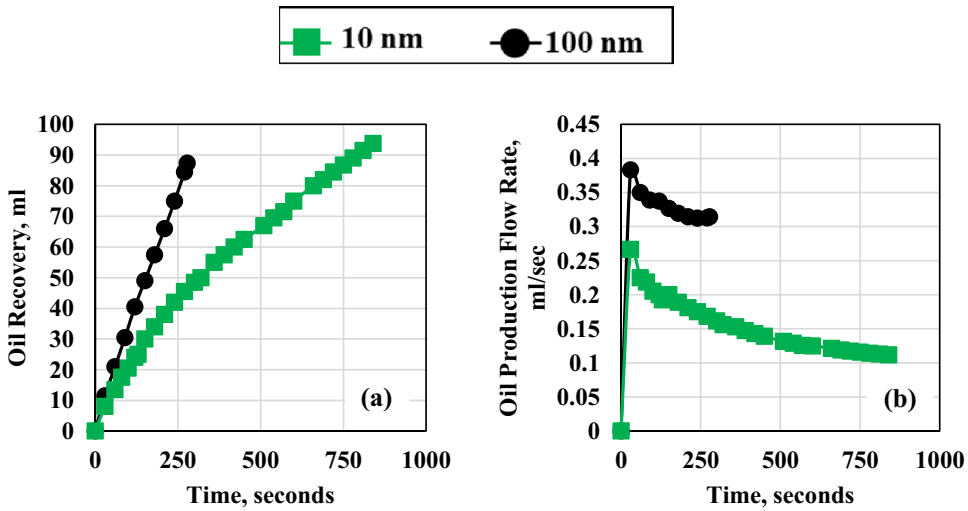

Fig. 5 Comparing 100 nm and 10 nm **a** oil production with time, and **b** oil production flow rate with time

trend is related to both pore sizes exhibiting the same flow regime based on their calculated Knudsen number, shown in Table 3.

6.1.5 Porous media thickness

All of the experiments in this research were conducted using a uniform thickness filter membrane. As the thickness of the membrane increases, it become more difficult for the CO_2 to mobilize the oil, and also the oil begins adsorbing to the filter membrane surface, and thus production decreases, and the flow behavior changes. Three different filter paper thicknesses were used in this study, including 0.11 mm, 0.55 mm, and 1.1 mm. The experiments were conducted using 50 psi injection pressure, and 119 cp oil viscosity. Figure 6 shows all the results obtained using the three different filter paper thicknesses.

The increase in the filter paper thickness resulted in a decrease in the oil production and an increase in the gas breakthrough time. The average oil production flow rate also decreased significantly with the increase in filter paper thickness. When the filter membrane was recovered, a relatively large volume of the oil was found to have adsorbed to the pores of the membrane, which is one of the main reasons behind the decrease in the oil production. The oil that was adsorbed to the filter paper was composed of a high percentage of asphaltenes which indicates that the asphaltene will result in a high plugging of the pore space of the porous media.

6.2 Asphaltene precipitation and deposition

6.2.1 Filter cake formation and thickness

This section will elaborate on both the CO_2 production mechanism in the 2.7 µm filter membrane experiments, explained above, and will also show the significance of the precipitation and deposition of asphaltene, and the impact that both the CO_2 injection pressure and oil viscosity have on both the production mechanism and the asphaltene deposition.

The oil production flow rate was calculated by dividing the recovered volume by the time. Two major things can be derived from the flow rate curves. The first main finding is stability of the production flow rate for each oil viscosity and each CO_2 injection pressure. This can be seen in Fig. 7. The initial flow rate for all the plots is extremely high compared to the other flow rates; this is the time at which the CO_2 began mobilizing the oil and hence the largest flow rate is observed; following this point, the flow rate then begins to reach stabilization. The longer the duration of the production, the more time the flow had time to stabilize. The plots for the 63.7 cp, for example, appear to be unstable compared to the plots for the other oil viscosities that took a longer duration to produce.

A relationship between the average oil production flow rate, the overall oil production, and the CO_2 breakthrough pressure is shown in Table 2. As the CO_2 breakthrough time decreases, the oil production increases for each oil viscosity. Also, the decrease in CO_2 breakthrough time results in a larger average oil flow rate for the same viscosity oil. This shows that as the overall time for production decreases there is a higher average flow rate which in turn does not allow for the formation of a thick filter cake. This decrease in time occurs either with

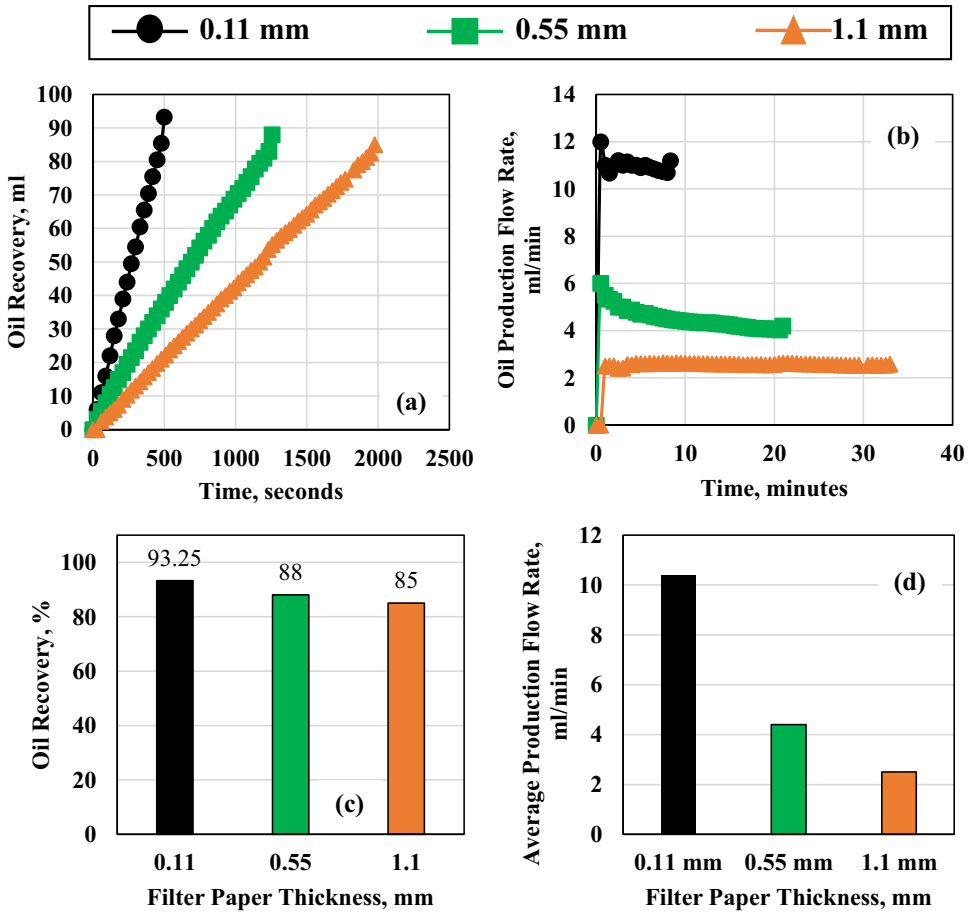

Fig. 6 Filter paper thickness effect on **a** gas breakthrough time, **b** oil production flow rate, **c** oil production, and **d** average production flow rate

the increase in CO_2 injection pressure or decrease in oil viscosity; the former has an effect on the oil production behavior, while the latter has an effect on the reduction in asphaltene concentration.

6.2.2 Asphaltene weight percent

The wt% of asphaltene was measured for all the experiments conducted. For each experiment, an oil sample was taken from the produced oil, and the filter cake, and the asphaltene weight percent was calculated using the Asphaltene Detection Test, explained before. The asphaltene weight percent for the original crude oil before running the filtration experiments is shown in Table 3 for reference.

Table 4 shows the asphaltene weight percent for the filtered oil and the filter cake samples for different viscosity oils, different pressures, and different pore sizes. For the 469 cp oil, increasing the pressure resulted in an increase in the asphaltene wt% in the filtered oil due to the oil being forced through the pores. With the decrease in viscosity, the asphaltene wt% also decrease. This is due to the initial asphaltene wt% being less in the less viscosity oil, as shown in Table 3. When the pore size was decreased, the filtered oil had a lower asphaltene wt%, which indicates that the asphaltene was harder to extrude through the smaller pore, even at a higher CO_2 injection pressure. For all the experiments, as the asphaltene wt% decreases in the filtered oil, it increases in the filter cake, since the concentration of asphaltene becomes higher due to a lower percentage passing though the filter membrane. These results validate the results obtained for the filter cake thickness above, with the highest filter cake thickness showing the highest asphaltene filter cake wt%.

7 Conclusions

This research studies the flow mechanism of CO_2 through nano and micro pores and the impact of this flow on oil mobilization and asphaltene instability in the crude oil. Based on the Knudsen number calculations, it was found that multiple flow regimes may arise during CO_2 flow in nano and micro pores; this reveals that diffusion is not necessarily the sole, or even the dominant, flow regime for CO_2 flow in nanopores. With the decrease in pore size, the oil recovery potential decreased, and the asphaltene damage and plugging increased significantly. This

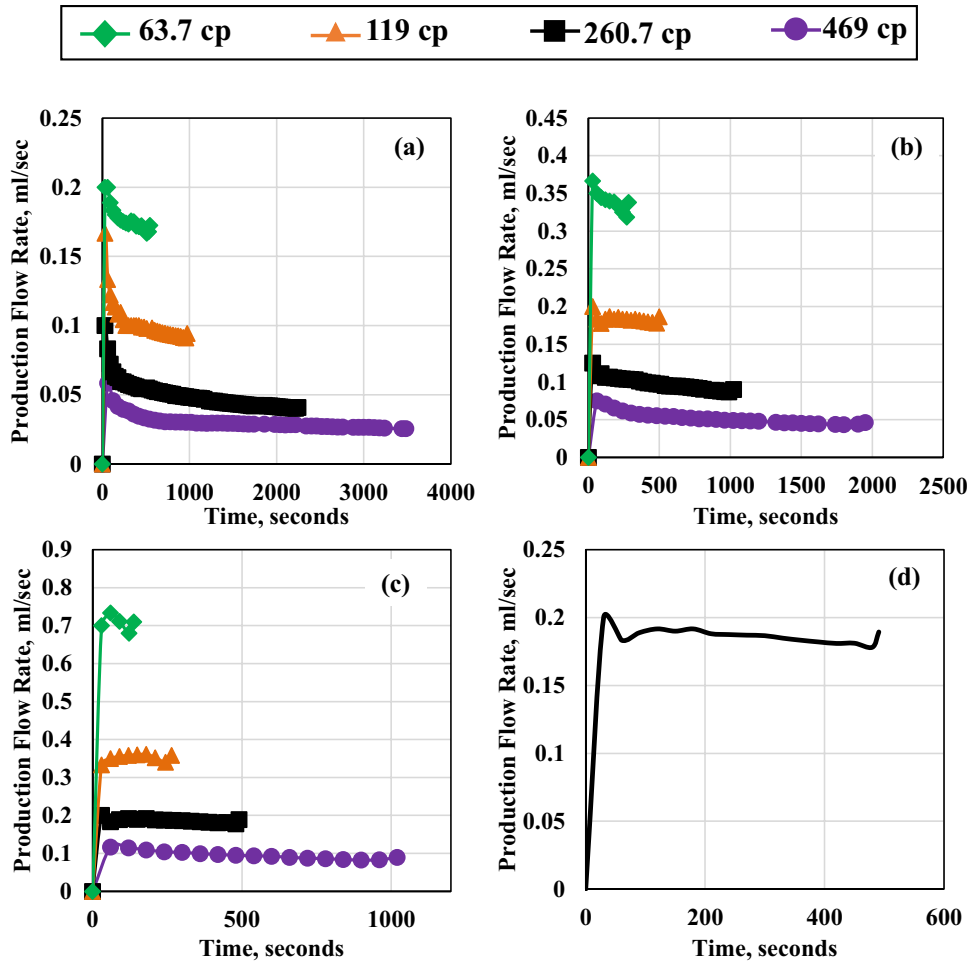

Fig. 7 Oil production flowrates for CO_2 injection pressures of **a** 25 psi, **b** 50 psi, **c** 100 psi, **d** 100 psi, 260.7 cp

Table 2 Values for experiments using 2.7 µm filter paper

Oil viscosity, cp	CO_2 injection pressure, psi	Oil production, %	CO_2 breakthrough time, s	Average production flow rate, ml/min
469	25	89	3340	1.79
469	50	90	1900	3.02
469	100	91	961	5.42
260.7	25	91.5	2220	2.94
260.7	50	92	990	5.71
260.7	100	93	480	10.58
119	25	92	960	5.97
119	50	93.25	480	10.39
119	100	95	244	19.02
63.7	25	94	530	10.11
63.7	50	96	270	18.53
63.7	100	98	122	35.35

was evident from the increase in pressure requirement to mobilize the crude oil through the filter membranes with nano pore sizes. Change in pressure was found to impact the oil recovery and the asphaltene plugging; this was due to the pressure's impact on the flow regime which was determined using Knudsen number. The CO_2 breakthrough time was decreased significantly when the oil viscosity was decreased due to the CO_2 being able to mobilize the lighter crude oil much easier than the heavy crude oil. Although the Knudsen number allows for the

Table 3 Asphaltene wt% for all the oil viscosities

Oil viscosity, cp	Asphaltene weight percent, %
469	5.73
260.7	4.63
119	4.01
63.7	3.22

Table 4 Asphaltene Wt% for The Filtered Oil and The Filter Cake

Oil viscosity, cp	Pressure, psi	Pore size	Filtered oil asphaltene wt%	Filter cake asphaltene wt%
469	25	2.7 µm	4.2	16
469	50	2.7 µm	4.4	14
469	100	2.7 µm	4.6	12
260.7	50	2.7 µm	3.8	12
119	50	2.7 µm	3.6	10
63.7	50	2.7 µm	2	6
469	300	100 nm	2.2	18
469	300	10 nm	1.3	23

prediction of the flow regime, it does not consider reservoir heterogeneity or tortuosity, which is one of the limitations of this research. Also, since the filter membranes are extremely thin and uniform in pore size, the heterogeneity was not incorporated in the porous media. These effects will be considered in future experiments along with a more detailed characterization of asphaltene propagation and interaction with CO_2.

Acknowledgements The corresponding author wishes to thank Missouri University of Science and Technology for its support through the Chancellors Distinguished Fellowship.

Compliance with ethical standards

Conflict of interest The authors declare that they have no conflict of interest.

References

1. Fakher S, Imqam A (2020) Application of carbon dioxide injection in shale oil reservoirs for increasing oil recovery and carbon dioxide storage. Fuel. https://doi.org/10.1016/j.fuel.2019.116944
2. Fakher S et al (2020) Hydrolyzed polyacrylamide—Fly ash reinforced polymer for chemical enhanced oil recovery: Part 1—Injectivity experiments. https://doi.org/10.1016/j.fuel.2019.116310.
3. Fakher S et al (2018) Investigating the viscosity reduction of ultra-heavy crude oil using hydrocarbon soluble low molecular weight compounds to improve oil production and transportation. Soc Pet Eng. https://doi.org/10.2118/193677-MS
4. Fakher S et al (2019) A characterization of different alkali chemical agents for alkaline flooding enhanced oil recovery operations: an experimental investigation. SN Appl Sci 1:1622. https://doi.org/10.1007/s42452-019-1662-2
5. Fakher S et al (2019) Carbon dioxide injection pressure and reservoir temperature impact on oil recovery from unconventional shale reservoirs during cyclic CO_2 injection: an experimental study. Carbon management technology conference. https://doi.org/10.7122/CMTC-558561-MS
6. Shabro V et al (2012) Forecasting gas production in organic shale with the combined numerical simulation of gas diffusion in Kerogen, Langmuir desorption form Kerogen surfaces, and advection in nanopores. In: Presented at the 2012 SPE annual technical conference and exhibition, San Antonio, Texas, USA, 8–10 Oct
7. Okamoto N et al (2015) Slip velocity and permeability of gas flow in nanopores for shale gas development. In: Presented at the SPE Asia Pacific unconventional resources conference and exhibition, Brisbane, Australia, 9–11 Nov
8. Okamoto N et al (2018) Slip velocity of methane flow in nanopores with Kerogen and Quartz surfaces. SPE J
9. Negara A et al (2016) Effects of multiple transport mechanisms on shale gas production behavior. In: Presented at the SPE Kingdom of Saudi Arabia annual technical symposium and exhibition, Dammam, Saudi Arabia, 25–28 April
10. Wu K et al (2016) A unified model for gas transfer in nanopores of shale-gas reservoirs: coupling pore diffusion and surface diffusion. SPE J
11. Xu J et al (2017) Nanoscale free gas transport in shale rocks: a hard-sphere based model. In: Presented at the SPE unconventional resources conference, Alberta, Canada, 15–16, Feb
12. Jin L et al (2017) Improving oil recovery by use of carbon dioxide in the Bakken unconventional system: a laboratory investigation. Soc Pet Eng. https://doi.org/10.2118/178948-PA
13. Li J et al (2017) Methane transport through nanoporous shale with sub-irreducible water saturation. In: Presented at the SPE Europec 79th EAGE conference and exhibition, Paris, France, 12–15 June
14. Zendehboudi S et al (2014) Asphaltene precipitation and deposition in oil reservoirs—Technical aspects, experimental and hybrid neural network predictive tools. Chem Eng Res Des 92(5):857–875
15. Fakher S et al (2019) Critical review of asphaltene properties and factors impacting its stability in crude oil. J Petrol Explor Prod Technol. https://doi.org/10.1007/s13202-019-00811-5
16. Fakher S, Imqam A (2020) A review of carbon dioxide adsorption to unconventional shale rocks methodology, measurement, and calculation. SN Appl Sci 2:5. https://doi.org/10.1007/s42452-019-1810-8
17. Fakher S (2019) Investigating factors that may impact the success of carbon dioxide enhanced oil recovery in shale reservoirs. Soc Petrol Eng. https://doi.org/10.2118/199781-STU
18. Fakher S (2019b) Asphaltene stability in crude oil during carbon dioxide injection and its impact on oil recovery: a review, data analysis, and experimental study. Masters Theses. 7881
19. Fakher S et al (2019) An experimental investigation of asphaltene stability in heavy crude oil during carbon dioxide injection. J Petrol Explor Prod Technol. https://doi.org/10.1007/s13202-019-00782-7
20. Rassamdana HB et al (1996) Asphaltene flocculation and deposition: I The onset of precipitation. AIChE J 42(1):10–22

21. Soroush S et al (2014) A comparison of asphaltene deposition in miscible and immiscible carbon dioxide flooding in porous media. Soc Petrol Eng. https://doi.org/10.2118/169657-MS
22. Kalantari-Dahagi A et al (2006) Formation damage due to asphaltene precipitation resulting from CO_2 gas injection in Iranian carbonate reservoirs. Soc Petrol Eng. https://doi.org/10.2118/99631-MS
23. Shedid and Zekri (2006) Formation damage caused by simultaneous sulfur and asphaltene deposition. Soc Petrol Eng. https://doi.org/10.2118/86553-PA
24. Tavakkoli M et al (2011) Prediction of asphaltene precipitation during solvent/CO_2 injection conditions: a comparative study on thermodynamic micellization model with a different characterization approach and solid model. Soc Petrol Eng J Can Petrol Technol. https://doi.org/10.2118/145638-PA
25. Yonebayashi H et al (2011) Dynamic asphaltene behavior for gas-injection risk analysis. Soc Petrol Eng Reserv Eval Eng J. https://doi.org/10.2118/146102-PA
26. Yonebayashi H et al (2018) Determination of asphaltene-onset pressure using multiple techniques in parallel. Soc Petrol Eng Prod Oper J. https://doi.org/10.2118/181278-PA
27. Moradi S et al (2012) Investigation of asphaltene precipitation in miscible gas injection processes: experimental study and modeling. Braz J Chem Eng 29(3):665–676
28. Struchkov et al (2019) Laboratory investigation of asphaltene-induced formation damage. doi.org/10.1007/s13202-018-0539-z
29. Shen and Sheng (2018) Experimental and numerical study of permeability reduction caused by asphaltene precipitation and deposition during CO_2 huff and puff injection in Eagle Ford shale. Fuel 211:432–445. https://doi.org/10.1016/j.fuel.2017.09.047
30. Fakher S, Imqam A (2018) Investigating and mitigating asphaltene precipitation and deposition in low permeability oil reservoirs during carbon dioxide flooding to increase oil recovery. Soc Petrol Eng. https://doi.org/10.2118/192558-MS
31. Fakher S, Imqam A (2019) Asphaltene precipitation and deposition during CO_2 injection in nano shale pore structure and its impact on oil recovery. https://doi.org/10.1016/j.fuel.2018.10.039.
32. Mohammed R et al (2017) Simulation study of asphaltene deposition and solubility of CO_2 in the brine during cyclic CO_2 injection process in unconventional tight reservoirs. Int J Geol Environ Eng 11(6):485–500
33. Fakher S et al (2019) The effect of unconventional oil reservoirs' nano pore size on the stability of asphaltene during carbon dioxide injection. Carbon management technology conference. https://doi.org/10.7122/CMTC-558486-MS
34. Goual L (2012). Petroleum Asphaltenes, crude oil emulsions- composition stability and characterization. ISBN: 978-953-51-0220-5
35. Shahriar M (2014) The aggregation of asphaltene molecules as a function of carbon dioxide concentration (PhD Dissertation). Texas Tech University
36. Ziarani AS, Aguilera R (2012) Knudsen's permeability correction for tight porous media. Transp Porous Med 91(1):239260. https://doi.org/10.1007/s11242-001-9842-6
37. Eide Ø (2016) Visualization of carbon dioxide enhanced oil recovery by diffusion in fractured chalk. Soc Petrol Eng. https://doi.org/10.2118/170920-PA
38. Knudsen M (1909) Die Gesetze der Molukularstrommung und der inneren. Reibungsstrornung der Gase durch Rohren. Ann der Phys 28:75–130
39. Karniadakis G (2005) Microflows and nanoflows: fundamentals and simulation. Springer, New York
40. Roy S et al (2003) Modeling gas flow through microchannels and nanopores. J Appl Phys 93:4870–4879
41. Beskok A, Karniadakis GE (1999) A model for flows in channels, pipes, and ducts at micro and nano scales. Nanoscale Microscale Thermophys Eng 3:43–77
42. Forchheimer P (1901) Wasserbewegug durch Boden. Zeits V Deutsch Ing 45:1782–1788
43. Klinkenberg LJ (1941) The permeability of porous media to liquid and gases. In: Paper presented at the API 11th mid year meeting, Tulsa. API Drilling and Production Practices, New York, pp 200–213
44. Maxwell JC (1867) On stresses in rarefied gases arising from inequalities of temperature. Phil Trans R Soc Lond 170:231–256
45. Knudt A, Warburg E (1875) Übwe Reibung and Wärmelei-tung verdünnter Gase. Poggendrfs Annalen der physic und Chemie 155:337
46. Sandler S (1972) Temperature dependence of the Knudsen permeability. Ind Eng Chem Fundam 11:424–427
47. Roque-Malherbe, R.M.A., 2007. Adsorption and Diffusion in Nanoporous Materials. CRC Press, Taylor & Francis Group, Boca Raton.
48. Lobanov et al. "Swelling/extraction test of Russian reservoir heavy oil by liquid carbon dioxide", 2018, doi.org/10.1016/S1876-3804(18)30095-8
49. Fakher S, Imqam A (2020) A simplified method for experimentally quantifying crude oil swelling during immiscible carbon dioxide injection. J Petrol Explor Prod Technol. https://doi.org/10.1007/s13202-020-00867-8
50. Fakher S (2020) Development of novel mathematical models for laboratory studies of hydrolyzed polyacrylamide polymer injectivity in high-permeability conduits. J Petrol Explor Prod Technol. https://doi.org/10.1007/s13202-020-00861-0
51. Fakher SM et al (2018) Enhancing carbon dioxide flooding sweep efficiency in high permeability hydrocarbon reservoirs using micro-particle gels. Soc Petrol Eng. https://doi.org/10.2118/192381-MS
52. Lawal KA, Crawshaw JP, Boek ES, Vesovic V (2012) Experimental investigation of asphaltene deposition in capillary flow. Energy Fuels 26(4):2145–2153. https://doi.org/10.1021/ef201874m
53. O Elkhatib, W Chaisoontornyotin, M Gesho, L Goual.. Nanoscale investigation of asphaltene deposition under capillary flow conditions. Energy & Fuels Article ASAP. 10.1021/acs.energyfuels.9b03504.
54. Boek ES, Ladva HK, Crawshaw JP, Padding JT (2008) Deposition of colloidal asphaltene in capillary flow: experiments and mesoscopic simulation. Energy Fuels 22(2):805–813. https://doi.org/10.1021/ef700670f
55. Ruiz-Morales Y, Mullins OC (2015) Coarse-grained molecular simulations to investigate asphaltenes at the oil–water interface. Energy Fuels 29(3):1597–1609. https://doi.org/10.1021/ef502766v